Hydrophilic mechano-bactericidal nanopillars require external forces to rapidly kill bacteria

Amin Valiei[1#], Nicholas Lin[1#], Jean-Francois Bryche[2,3], Geoffrey McKay[4], Michael Canva[2,3], Paul G. Charette[2,3], Dao Nguyen[4,5,6], Christopher Moraes[1,7,8]* and Nathalie Tufenkji[1]*

[1]Department of Chemical Engineering, McGill University, Montréal, Québec, Canada

[2]Laboratoire Nanotechnologies Nanosystèmes (LN2), CNRS UMI-3463, Université de Sherbrooke, Sherbrooke, Québec, Canada

[3]Institut Interdisciplinaire d'Innovation Technologique (3IT), Université de Sherbrooke, Sherbrooke, Québec, Canada

[4]Meakins-Christie Laboratories, Research Institute of the McGill University Health Centre, Montréal, Québec, Canada

[5]Department of Microbiology and Immunology, McGill University, Montréal, Québec, Canada

[6]Department of Medicine, McGill University, Montréal, Québec, Canada

[7]Department of Biomedical Engineering, McGill University, Montréal, Québec, Canada

[8]Rosalind and Morris Goodman Cancer Research Center, McGill University, Montréal, Québec, Canada

[#]Authors contributed equally

*Corresponding authors:

C. Moraes: chris.moraes@mcgill.ca; +1 514-398-4278

N. Tufenkji : nathalie.tufenkji@mcgill.ca; +1 514-398-2999

Abstract

Recently, nanopillars have been shown to mechanically damage bacteria, suggesting a promising strategy for future antibacterial surfaces. However, the mechanisms underlying this phenomena remain unclear, which ultimately limits translational potential towards real-world applications. Using real-time and end-point analysis techniques, we demonstrate that in contrast to initial expectations, bacteria on multiple hydrophilic “mechano-bactericidal” surfaces remained viable, unless exposed to a moving air-liquid interface, which caused considerable cell death. Reasoning that normal forces arising from surface tension may underlie this mechano-bactericidal activity, we developed computational and experimental models to estimate, manipulate, and recreate the impact of these forces. Our experiments together demonstrate that a critical level of external force acting on cells attached to nanopillar surfaces can rapidly deform and rupture bacteria. These studies provide fundamental physical insight into how nanopillar surfaces can serve as effective antibacterial materials, and suggest use-conditions under which such nanotechnology approaches may provide practical value.

Keywords: mechano-bactericidal, air-liquid interface, silicon nanopillars, zinc oxide nanopillars, surface tension, external force

Innovative antimicrobial technologies can play an important role in future designs of surfaces used in hospitals, public transportation, and food production equipment[1-3]. Disinfecting these surfaces through routine application of biocides risks the emergence of antimicrobial-resistant strains[4-5]. Surface immobilization of antibacterial compounds that kill on contact reduces diffusion of biocides, but has a limited lifetime as the compounds can degrade; and reduced antibacterial potency over time can promote the emergence of drug resistance[6]. To overcome these limitations, antibacterial approaches that rely on physical factors such as the surface's topography have recently been proposed as a strategy to maintain cost-effective bactericidal efficiency, thereby circumventing evolutionary mechanisms that give rise to drug resistance.

In 2012, Ivanova et al. reported that nanopillars on the wings of the *Psaltodo claripennis* cicada insect are capable of structurally deforming bacteria and are therefore considered antibacterial[7]. Changing the surface chemistry of the cicada wing did not alter antibacterial effectiveness, implying that bactericidal activity of natural nanopillar arrays originates from physical interactions that can deform and rupture the bacterial cell membrane[8]. Subsequent studies showed similar nanopillar-mediated antibacterial behaviour on the wings of other insects, such as damselflies and dragonflies, which have sharper nanopillars said to deliver even higher antibacterial efficacy[9-10]. These initial discoveries prompted the development of engineered nanopillars capable of mimicking this physical antibacterial mechanism, such as black silicon nanopillars that mimic nanopillars of dragonfly wings with remarkable bactericidal activity[11]. Nanopillars constructed from titanium[12], chitosan[13], stainless steel[14], zinc oxide[15], zinc phthalocyanine[16], poly(methyl methacrylate)[17], carbon nanotubes[18] and others have also shown antibacterial capabilities[19-22]. The diversity of these materials reinforces the notion that the

dominant antibacterial mechanism originates from physical structure rather than chemical interactions.

While past works confirm that mechanical forces are responsible for damaging bacteria on nanopillars[20-21], there is no consensus on the mechanism(s) of action of the killing forces involved. For instance, mechanical damage caused by nanopillars has been attributed by some researchers to adhesion forces which deform cells upon contact with the nanopillars[8, 19]. Alternatively, bacteria may be killed by shear forces generated when attached cells attempt to move laterally on nanopillars[23-24], or when bending energy stored in flexible, high aspect ratio nanopillars is released[25]. Surface properties such as wettability of the nanopillars also appear to play a role[26]. Hence, it seems likely that multiple mechanisms of mechano-bactericidal activity are possible, and are dependent on factors such as surface chemistry, nanopillar geometries, and bacterial incubation conditions. In this work, we evaluate the importance of external forces that may be applied either by design or inadvertently, to drive rapid cell death on nanopillar surfaces.

To evaluate a potential role for external mechanical forces, we studied nanopillar-mediated bacterial killing efficiency of multiple hydrophilic nanopillar surfaces fabricated from etching of silicon (NanoSi), self-assembly of zinc oxide (NanoZnO), nanolithography of silicon, as well as natural cicada wings to encompass a large range of nanopillar geometries[27]. NanoSi and NanoZnO surfaces were used as the primary test surfaces for this study, as both can be controllably fabricated at high throughput to support multiple experiments and conditions. Furthermore, NanoSi is well-studied in the context of mechano-bactericidal surfaces and shows the highest antibacterial performance reported[11, 20] whereas the hydrothermal synthesis of NanoZnO is well-established in the literature. Morphology of the nanopillars was characterized by scanning electron microscopy (SEM) (Fig. 1). Nanopillars of NanoSi are generally tapered, sharper and narrower than nanopillars

of NanoZnO, which are blunt-ended and wider. The dimensions of the nanopillars (Table S1) were synthesized to be within the range of previously reported mechano-bactericidal structures (Table 4 in Lin *et al.*[22] and Table 2 in Tripathy *et al.*[20]). Fabrication and characterization details for all surfaces are available in the Supporting Information (SI).

The model bacterium chosen for this study was *Pseudomonas aeruginosa,* a Gram-negative bacterium known to be a key causative agent of opportunistic human infections[28]. Viability of *P. aeruginosa* was initially evaluated on both NanoSi and NanoZnO nanopillar surfaces while fully immersed in a bacterial suspension labeled with a mixture of live (SYTO 9; green) and dead (propidium iodide; red) fluorescent dyes. Other studies demonstrate mechano-bactericidal activity within f3-5 minutes, and up to 18 hours of incubation[7,23-24,29] on similar surfaces. In our hands, we detected no antibacterial activity even up to 24 hours provided that the nanopillar surfaces were maintained in submerged culture conditions. Fluorescently-labelled motile *P. aeruginosa* adhered to both surfaces immediately but the vast majority of cells (>98%) remained viable after 1 h (Fig. 2b and Fig. S1a). At 24 hours, bacteria progressed towards forming a biofilm and there was still no appreciable loss in the viability of attached bacteria (Fig. S1b).

To reconcile our experimental results with those of others, we then wondered whether aspects of our experimental handling may resolve these discrepancies. We first noted that in our hands, although the bacterial suspension appeared to wet the surfaces, we occasionally found randomly entrapped microscopic air bubbles that could be quickly eliminated by gentle agitation similar to previous reports in small-scale experiments[30-31]. If not eliminated, these air bubbles may spontaneously expand during microscopy. To our surprise, we observed substantial bacterial killing within the expansion zone while the cells outside the air bubble remained viable (Fig. S2), suggesting that the air-liquid interface could play an important role in this process.

To better understand how a moving air-liquid interface on a nanopillar surface might affect bacterial viability, we dispensed a 3 μL droplet of bacterial suspension on the nanopillar surfaces and monitored the droplet under fluorescent microscopy. Initially, all attached and planktonic cells observed under the microscope were viable (Fig. 2a, t = 0). The droplet volume decreased rapidly due to evaporation which caused the air-liquid interface to recede from the edge towards the droplet center. Monitoring the location where the contact line was passing (represented by a yellow line in Fig. 2a, t = 30 s), we observed that (i) bacteria were not swept away by the droplet interface but were left behind on the nanopillar surfaces; and (ii) they began to uptake cell membrane-impermeable propidium iodide rapidly after air-liquid interface passage (Fig. 2a; t = 60, 90 s), indicating cell death. Over 99.9% of the bacteria on NanoSi (Fig. 2a; t=120 s, Fig. 2c) and over 90% on NanoZnO (Fig. S3, 2c) stained positive for propidium iodide. In contrast, over 95% of attached bacteria on flat surfaces remained viable even after all liquid evaporated, confirming that this phenomenon is specific to the nanopillar topographies (Fig. 2a,b) and not a result of bacterial dessication or increase in salinity during evaporation. We further confirmed that the results were not an artefact related to the dyes by studying the green fluorescent protein (GFP) signal loss upon air-liquid interface displacement of GFP-tagged *P. aeruginosa* instead of viability staining (Fig. S4).

The live/dead assay provides information on the integrity of the cell membrane but does not capture morphological damage on the nanopillar surfaces. We therefore used SEM to investigate bacterial structure associated with the live/dead state. As before, a droplet of bacterial suspension was partially dried on each nanopillar surface, and to protect the sample integrity in the just-dried state, the samples were immediately chemically-fixed by glutaraldehyde and prepared for SEM by critical point drying (CPD). CPD retains bacterial morphology during drying by gradually

replacing the liquid medium with liquid CO_2 which is later discharged at supercritical conditions without surface tension effects to distort cell morphology[32]. Carefully following these sample preparation steps allowed us to confirm that bacteria only showed significant cell deformation and damage in the just-dried state on nanopillar surfaces; while bacterial integrity remained intact on control (flat) surfaces or when maintained in fully immersed conditions throughout sample handling (Fig. 3, S5). This is consistent with our live/dead assays previously described (Fig. 2b, S1), strongly suggesting that the passage of an air-liquid interface is required to generate rapid antibacterial activity on nanopillars.

To confirm that these surprising findings are not restricted to NanoSi and NanoZnO, we conducted further proof-of-concept studies on other surfaces previously reported to have mechano-bactericidal properties, including cicada wings of the species *Salvazana mirabilis* as well as highly ordered silicon nanopillars fabricated to minimize geometric variability[27]. Again, SEM observations show cells were damaged on these nanopillar surfaces upon water evaporation, but not in the wet condition (Fig. S6), suggesting that this phenomenon may potentially extend to surfaces with different geometric features and wettabilities.

Given that the movement of an air-liquid interface is a requirement for the observed bactericidal activity in our hands, we reasoned that the substantial normal forces associated with an air-liquid interface[33] exerted by the capillary action of fluids might be responsible for rupturing bacteria on the nanopillars. To test this hypothesis, we first estimated the magnitude of normal capillary forces during water evaporation using computational approaches, and then experimentally validated this mechanism by manipulating physical parameters associated with normal forces.

Capillary forces arise when the evaporating liquid level falls below the bacterial cell height (Fig. 4a). The first component of the capillary forces is the surface tension force ($\mathbf{F_s}$) which acts around the periphery of the meniscus along the liquid/vapor interface[34-35]. $\mathbf{F_s}$ is calculated using:

$$\mathbf{F}_s = \int_C \boldsymbol{\gamma} dl \quad \text{(Eq. 1)}$$

Where γ is the surface tension and C is the perimeter of the contact line. Assuming a constant contact angle between the thin liquid film and bacterium during evaporation[36], the integral of vertical component of the surface tension around the contact line yields the vertical force along the z-axis ($F_{s,z}$). Assuming an idealized cylindrical bacterium geometry with two hemispherical caps, the magnitude of this force is:

$$F_{s,z} = 2\gamma(\pi R\sin\alpha + L)\sin(\alpha + \theta) \quad 0 \le \alpha \le \pi \quad \text{(Eq. 2)}$$

Where L is the length of the cylindrical part of the bacterium, R is the radius of the hemispherical edge of the bacterium, θ is the contact angle of the liquid with the bacterial surface, and α is the falling angle describing the position of three-phase contact line on the hemispherical end of a bacterium. The second component of normal capillary forces is caused by pressure differentials across the curved liquid/air interface. We experimentally determined that both surfaces were highly hydrophilic, with water droplet contact angles of 5° and 20° respectively for NanoSi and NanoZnO. Since these values are low, the droplet interface is nearly flat, and hence contributes only a small pressure differential across the interface, maximizing the downward force by eliminating the effect of opposing capillary pressure. Wicking of liquid between nanopillars ensures that this condition remains valid during the evaporation timecourse36[37]. Substituting L~1.0 μm, R~250 nm, γ=72 mN/m[38] in Eq. 2, $F_{s,z}$ was calculated for $\alpha_0 < \alpha < \pi$ where α_0 is the initial equilibrium position based on the flat interface assumption and $\pi/6 < \theta < \pi/2$ which covers the range of bacterial surface contact angles reported for *P. aeruginosa*[39-41]. For each value of θ, $F_{s,z}$

increases as water evaporates (*H*, liquid level, decreases), reaches a maximum value, and then decreases (Fig. 4b). The maximum value of $F_{s,z}$ is between 150 nN and 250 nN for the above range of contact angles.

To determine whether these forces are sufficient to stress the bacterial cell wall to the point of rupture, we simulated the cell wall in contact with a nanopillar under an "external" load to capture surface tension forces in a lumped parameter model (Fig. 4c). This model shows that a normal force of ~1.1 nN/pillar for NanoSi and ~ 6.7 nN/pillar for NanoZnO is required to exceed the cell envelope ultimate tensile strength (Fig. S7). The normal capillary forces at the air-liquid interface approach ~7× the critical force to rupture the cell wall for NanoSi and ~4× for NanoZnO (Fig. S9; assuming that ~20 NanoSi pillars and ~6 NanoZnO pillars are in contact with each cell, with equal reaction forces from each of the pillars). Hence, the external forces generated by the air-liquid interface are theoretically large enough to rupture bacterial cells on nanopillars.

This computational model has intrinsic limitations, including an inability to capture nanopillar or cell wall heterogeneity, or complexity of the cell-surface interaction. The model does however allow us to demonstrate that surface tension is a critical feature as the capillary force is linearly dependent on the magnitude of surface tension. Therefore, to experimentally validate the model, we manipulated surface tension properties by adding a surfactant to the test solution. Tween80 surfactant at 0.5 wt% concentration reduces the water surface tension by approximately 65%, and is nontoxic to *P. aeruginosa* at this concentration in submerged conditions. Adding surfactant significantly reduced the antibacterial efficacy of the nanopillars upon drying by ~74% on NanoZnO and ~20% on NanoSi (Fig. 4d). Hence, reducing the surface tension and consequently the applied normal forces during air-liquid interface movement rescues bacterial viability, demonstrating that a critical external load is required for mechano-bactericidal activity.

Finally, to confirm that normal forces specifically are responsible for the bactericidal phenomenon, we applied external compressive loads to directly deliver normal forces to bacterial cells on the nanopillars. A weighted 3D-printed stamp featuring an array of circular posts was pressed against NanoSi or NanoZnO surfaces while immersed in the bacterial suspension (Fig. 5a). The apparent stress (σ) delivered to each surface was calculated based on the weight used to load the stamps against the surface. On flat control samples, all cells remained viable at the highest applied stress in this experiment. For areas of the NanoSi or NanoZnO surfaces that made contact with the stamp's posts, circular regions of dead bacteria were produced for sufficiently high applied stresses while no cell death was observed in the regions between the compressive pillars (Fig. 5b,c). Stresses as low as 0.17 MPa can produce a kill region on NanoSi but not on NanoZnO, which required a larger stress (0.4 MPa and above) to achieve the same antibacterial effect (Fig. 5d). This correlates well with our earlier observations demonstrating that nanopillars of NanoSi and NanoZnO alone cannot drive bacterial death, but that a coupled external force with the nanopillar surface is necessary to deliver critical cell damage.

The identification of external forces as an effective strategy to achieve rapid mechano-bactericidal activity has important implications for research of mechano-bactericidal effects, both in designing experiments for nanopillar surfaces or in devising novel applications for these technologies. We demonstrate that the described external normal forces can kill bacteria within seconds, which may be of pratical utility compared to other proposed mechanisms (e.g. 3-5 min to 18 h reported for adhesion [7-29], and 10 min to 2 h for motility[23-24]). These findings therefore suggest practical applications where this mechanism might be employed, including designing antibacterial surfaces for healthcare environments that are high-touch, or are normally dry but are expected to be occasionally exposed to droplets contaminated with pathogens. Alternatively, for applications

requiring antibacterial properties in submerged conditions, such as anti-biofouling materials in industry or medical implants, a controllable external force may be implemented to enhance mechano-bactericidal action. Designing systems to create these forces in conjunction with nanopillar structures should hence be an important research topic in designing topographical materials for practical antibacterial activity.

These findings also highlight the importance of ensuring that experimental protocols explicitly control for air-liquid interface passage or other artefacts that may generate such forces; particularly given the capacity for nanopillars to entrap air bubbles, and increased rates of evaporation noted on hydrophilic nanopillar surfaces compared to flat control surfaces (Fig. S10). Similarly, sample transfer and rinsing steps may also inadvertently apply sufficient external forces to kill bacteria on nanopillars, through the formation of a temporary air-liquid interface.

In summary, we fabricated hydrophilic nanopillar surfaces and exposed them to the bacterium *P. aeruginosa*. No antibacterial activity was observed for up to 24 hours when maintained in submerged culture. However, passage of an air-liquid interface, either through evaporation or an expanding air pocket, caused rapid cell death. We then computationally and experimentally demonstrated that normal forces associated with these events are sufficient to kill bacteria on nanopillars. Finally, we verified that sufficiently large external normal forces can efficiently kill bacteria on NanoSi and NanoZnO while maintaining fully submerged conditions. These findings therefore establish that for hydrophilic nanopillar surfaces, external forces provide a complementary mechanism to generate rapid mechano-bactericidal activity.

Acknowledgements

This research was supported, in part, thanks to funding from the Natural Sciences and Engineering Research Council of Canada (NSERC), the McGill Interdisciplinary Initiative in

Infection and Immunity (MI4) (NT, DN), the Canada Foundation for Innovation, the Canada Research Chairs program (NT, CM), the NSERC Discovery Grants program (CM, MC, PGC) and the McGill Engineering Doctoral Award (AV, NL). AV and NL each hold NSERC postgraduate scholarships. JFB is supported by the Fonds de recherche du Québec – Nature et technologies (FRQNT) and the Merit scholarship program for foreign students (n° 273433). LN2 is an international laboratory (Unité Mixte Internationale UMI 3463) jointly managed by French Centre national de la recherche scientifique and the Université de Sherbrooke as well as Université de Lyon (ECL, INSA de Lyon, CPE) and the Université Grenoble-Alpes (UGA). LN2 is also financially supported by FRQNT. We thank Dr. Reghan J. Hill for useful discussions. We are also grateful to the Advanced Bioimaging Facility and the Facility for Electron Microscopy Research at McGill University and CMC Microsystems for access to simulation software and to the Montréal Insectarium for providing cicada samples.

Conflicts of Interest

The authors declare no competing conflicts of interest.

References

1. Mattila-Sandholm, T.; Wirtanen, G., Biofilm formation in the industry: A review. *Food Reviews International* **1992,** *8* (4), 573-603.
2. Dancer, S. J., Controlling hospital-acquired infection: focus on the role of the environment and new technologies for decontamination. *Clinical microbiology reviews* **2014,** *27* (4), 665-690.
3. Malhotra, B.; Keshwani, A.; Kharkwal, H., Antimicrobial food packaging: potential and pitfalls. *Frontiers in microbiology* **2015,** *6*, 611.
4. Maillard, J. Y., Bacterial resistance to biocides in the healthcare environment: should it be of genuine concern? *Journal of Hospital Infection* **2007,** *65*, 60-72.
5. Mah, T.-F. C.; O'toole, G. A., Mechanisms of biofilm resistance to antimicrobial agents. *Trends in microbiology* **2001,** *9* (1), 34-39.
6. Hasan, J.; Crawford, R. J.; Ivanova, E. P., Antibacterial surfaces: the quest for a new generation of biomaterials. *Trends in Biotechnology* **2013,** *31* (5), 295-304.
7. Ivanova, E. P.; Hasan, J.; Webb, H. K.; Truong, V. K.; Watson, G. S.; Watson, J. A.; Baulin, V. A.; Pogodin, S.; Wang, J. Y.; Tobin, M. J.; Löbbe, C.; Crawford, R. J., Natural Bactericidal Surfaces: Mechanical Rupture of Pseudomonas aeruginosa Cells by Cicada Wings. *Small* **2012,** *8* (16), 2489-2494.
8. Pogodin, S.; Hasan, J.; Baulin, V. A.; Webb, H. K.; Truong, V. K.; Phong Nguyen, T. H.; Boshkovikj, V.; Fluke, C. J.; Watson, G. S.; Watson, J. A.; Crawford, R. J.; Ivanova, E. P., Biophysical model of bacterial cell interactions with nanopatterned cicada wing surfaces. *Biophys J* **2013,** *104* (4), 835-40.
9. Mainwaring, D. E.; Nguyen, S. H.; Webb, H.; Jakubov, T.; Tobin, M.; Lamb, R. N.; Wu, A. H.; Marchant, R.; Crawford, R. J.; Ivanova, E. P., The nature of inherent bactericidal activity: insights from the nanotopology of three species of dragonfly. *Nanoscale* **2016,** *8* (12), 6527-34.
10. Truong, V. K.; Geeganagamage, N. M.; Baulin, V. A.; Vongsvivut, J.; Tobin, M. J.; Luque, P.; Crawford, R. J.; Ivanova, E. P., The susceptibility of Staphylococcus aureus CIP 65.8 and Pseudomonas aeruginosa ATCC 9721 cells to the bactericidal action of nanostructured Calopteryx haemorrhoidalis damselfly wing surfaces. *Appl Microbiol Biotechnol* **2017,** *101* (11), 4683-4690.
11. Ivanova, E. P.; Hasan, J.; Webb, H. K.; Gervinskas, G.; Juodkazis, S.; Truong, V. K.; Wu, A. H. F.; Lamb, R. N.; Baulin, V. A.; Watson, G. S.; Watson, J. A.; Mainwaring, D. E.; Crawford, R. J., Bactericidal activity of black silicon. *Nature Communications* **2013,** *4*, 2838.
12. Wandiyanto, J. V.; Cheeseman, S.; Truong, V. K.; Kobaisi, M. A.; Bizet, C.; Juodkazis, S.; Thissen, H.; Crawford, R. J.; Ivanova, E. P., Outsmarting superbugs: bactericidal activity of nanostructured titanium surfaces against methicillin- and gentamicin-resistant Staphylococcus aureus ATCC 33592. *Journal of Materials Chemistry B* **2019,** *7* (28), 4424-4431.
13. Tripathy, A.; Pahal, S.; Mudakavi, R. J.; Raichur, A. M.; Varma, M. M.; Sen, P., Impact of Bioinspired Nanotopography on the Antibacterial and Antibiofilm Efficacy of Chitosan. *Biomacromolecules* **2018,** *19* (4), 1340-1346.
14. Jang, Y.; Choi, W. T.; Johnson, C. T.; García, A. J.; Singh, P. M.; Breedveld, V.; Hess, D. W.; Champion, J. A., Inhibition of Bacterial Adhesion on Nanotextured Stainless Steel 316L by Electrochemical Etching. *ACS Biomaterials Science & Engineering* **2018,** *4* (1), 90-97.
15. Yi, G.; Yuan, Y.; Li, X.; Zhang, Y., ZnO Nanopillar Coated Surfaces with Substrate-Dependent Superbactericidal Property. *Small* **2018,** *14* (14), e1703159.

16. Gonzalez Arellano, D. L.; Kolewe, K. W.; Champagne, V. K.; Kurtz, I. S.; Burnett, E. K.; Zakashansky, J. A.; Arisoy, F. D.; Briseno, A. L.; Schiffman, J. D., Gecko-Inspired Biocidal Organic Nanocrystals Initiated from a Pencil-Drawn Graphite Template. *Scientific Reports* **2018,** *8* (1), 11618.
17. Dickson, M. N.; Liang, E. I.; Rodriguez, L. A.; Vollereaux, N.; Yee, A. F., Nanopatterned polymer surfaces with bactericidal properties. *Biointerphases* **2015,** *10* (2), 021010.
18. Kang, S.; Herzberg, M.; Rodrigues, D. F.; Elimelech, M., Antibacterial Effects of Carbon Nanotubes: Size Does Matter! *Langmuir* **2008,** *24* (13), 6409-6413.
19. Luan, Y.; Liu, S.; Pihl, M.; van der Mei, H. C.; Liu, J.; Hizal, F.; Choi, C.-H.; Chen, H.; Ren, Y.; Busscher, H. J., Bacterial interactions with nanostructured surfaces. *Current Opinion in Colloid & Interface Science* **2018,** *38*, 170-189.
20. Tripathy, A.; Sen, P.; Su, B.; Briscoe, W. H., Natural and bioinspired nanostructured bactericidal surfaces. *Advances in Colloid and Interface Science* **2017,** *248*, 85-104.
21. Modaresifar, K.; Azizian, S.; Ganjian, M.; Fratila-Apachitei, L. E.; Zadpoor, A. A., Bactericidal effects of nanopatterns: A systematic review. *Acta Biomaterialia* **2019,** *83*, 29-36.
22. Lin, N.; Berton, P.; Moraes, C.; Rogers, R. D.; Tufenkji, N., Nanodarts, nanoblades, and nanospikes: Mechano-bactericidal nanostructures and where to find them. *Advances in Colloid and Interface Science* **2018,** *252*, 55-68.
23. Bandara, C. D.; Singh, S.; Afara, I. O.; Wolff, A.; Tesfamichael, T.; Ostrikov, K.; Oloyede, A., Bactericidal Effects of Natural Nanotopography of Dragonfly Wing on Escherichia coli. *ACS Appl Mater Interfaces* **2017,** *9* (8), 6746-6760.
24. Jindai, K.; Nakade, K.; Masuda, K.; Sagawa, T.; Kojima, H.; Shimizu, T.; Shingubara, S.; Ito, T., Adhesion and bactericidal properties of nanostructured surfaces dependent on bacterial motility. *RSC Advances* **2020,** *10* (10), 5673-5680.
25. Linklater, D. P.; De Volder, M.; Baulin, V. A.; Werner, M.; Jessl, S.; Golozar, M.; Maggini, L.; Rubanov, S.; Hanssen, E.; Juodkazis, S.; Ivanova, E. P., High Aspect Ratio Nanostructures Kill Bacteria via Storage and Release of Mechanical Energy. *ACS Nano* **2018,** *12* (7), 6657-6667.
26. Nakade, K.; Jindai, K.; Sagawa, T.; Kojima, H.; Shimizu, T.; Shingubara, S.; Ito, T., Adhesion and Bactericidal Properties of a Wettability-Controlled Artificial Nanostructure. *ACS Applied Nano Materials* **2018,** *1* (10), 5736-5741.
27. Bhadra, C. M.; Werner, M.; Baulin, V. A.; Truong, V. K.; Kobaisi, M. A.; Nguyen, S. H.; Balcytis, A.; Juodkazis, S.; Wang, J. Y.; Mainwaring, D. E.; Crawford, R. J.; Ivanova, E. P., Subtle Variations in Surface Properties of Black Silicon Surfaces Influence the Degree of Bactericidal Efficiency. *Nano-Micro Letters* **2018,** *10* (2), 36.
28. Stover, C. K.; Pham, X. Q.; Erwin, A. L.; Mizoguchi, S. D.; Warrener, P.; Hickey, M. J.; Brinkman, F. S. L.; Hufnagle, W. O.; Kowalik, D. J.; Lagrou, M.; Garber, R. L.; Goltry, L.; Tolentino, E.; Westbrock-Wadman, S.; Yuan, Y.; Brody, L. L.; Coulter, S. N.; Folger, K. R.; Kas, A.; Larbig, K.; Lim, R.; Smith, K.; Spencer, D.; Wong, G. K. S.; Wu, Z.; Paulsen, I. T.; Reizer, J.; Saier, M. H.; Hancock, R. E. W.; Lory, S.; Olson, M. V., Complete genome sequence of Pseudomonas aeruginosa PAO1, an opportunistic pathogen. *Nature* **2000,** *406* (6799), 959-964.
29. Nguyen, D. H. K.; Loebbe, C.; Linklater, D. P.; Xu, X.; Vrancken, N.; Katkus, T.; Juodkazis, S.; Maclaughlin, S.; Baulin, V.; Crawford, R. J.; Ivanova, E. P., The idiosyncratic self-cleaning cycle of bacteria on regularly arrayed mechano-bactericidal nanostructures. *Nanoscale* **2019,** *11* (35), 16455-16462.

30. Pereiro, I.; Fomitcheva Khartchenko, A.; Petrini, L.; Kaigala, G. V., Nip the bubble in the bud: a guide to avoid gas nucleation in microfluidics. *Lab on a Chip* **2019,** *19* (14), 2296-2314.
31. Ramsingh, R.; Grygorczyk, A.; Solecki, A.; Cherkaoui, L. S.; Berthiaume, Y.; Grygorczyk, R., Cell deformation at the air-liquid interface induces Ca2+-dependent ATP release from lung epithelial cells. *Am J Physiol Lung Cell Mol Physiol* **2011,** *300* (4), L587-95.
32. Horridge, G. A.; Tamm, S. L., Critical point drying for scanning electron microscopic sthdy of ciliary motion. *Science* **1969,** *163* (3869), 817-8.
33. Tavana, H.; Zamankhan, P.; Christensen, P. J.; Grotberg, J. B.; Takayama, S., Epithelium damage and protection during reopening of occluded airways in a physiologic microfluidic pulmonary airway model. *Biomed Microdevices* **2011,** *13* (4), 731-42.
34. Marmur, A., Tip-surface capillary interactions. *Langmuir* **1993,** *9* (7), 1922-1926.
35. de Lazzer, A.; Dreyer, M.; Rath, H. J., Particle−Surface Capillary Forces. *Langmuir* **1999,** *15* (13), 4551-4559.
36. Kralchevsky, P. A.; Nagayama, K., Capillary forces between colloidal particles. *Langmuir* **1994,** *10* (1), 23-36.
37. Bico, J.; Thiele, U.; Quéré, D., Wetting of textured surfaces. *Colloids and Surfaces A: Physicochemical and Engineering Aspects* **2002,** *206* (1), 41-46.
38. Vargaftik, N. B.; Volkov, B. N.; Voljak, L. D., International Tables of the Surface Tension of Water. *Journal of Physical and Chemical Reference Data* **1983,** *12* (3), 817-820.
39. Vanhaecke, E.; Remon, J. P.; Moors, M.; Raes, F.; De Rudder, D.; Van Peteghem, A., Kinetics of Pseudomonas aeruginosa adhesion to 304 and 316-L stainless steel: role of cell surface hydrophobicity. *Applied and Environmental Microbiology* **1990,** *56* (3), 788-795.
40. Atabek, A.; Camesano, T. A., Atomic Force Microscopy Study of the Effect of Lipopolysaccharides and Extracellular Polymers on Adhesion of Pseudomonas aeruginosa. *Journal of Bacteriology* **2007,** *189* (23), 8503-8509.
41. Das, T.; Kutty, S. K.; Kumar, N.; Manefield, M., Pyocyanin facilitates extracellular DNA binding to Pseudomonas aeruginosa influencing cell surface properties and aggregation. *PLoS One* **2013,** *8* (3), e58299.

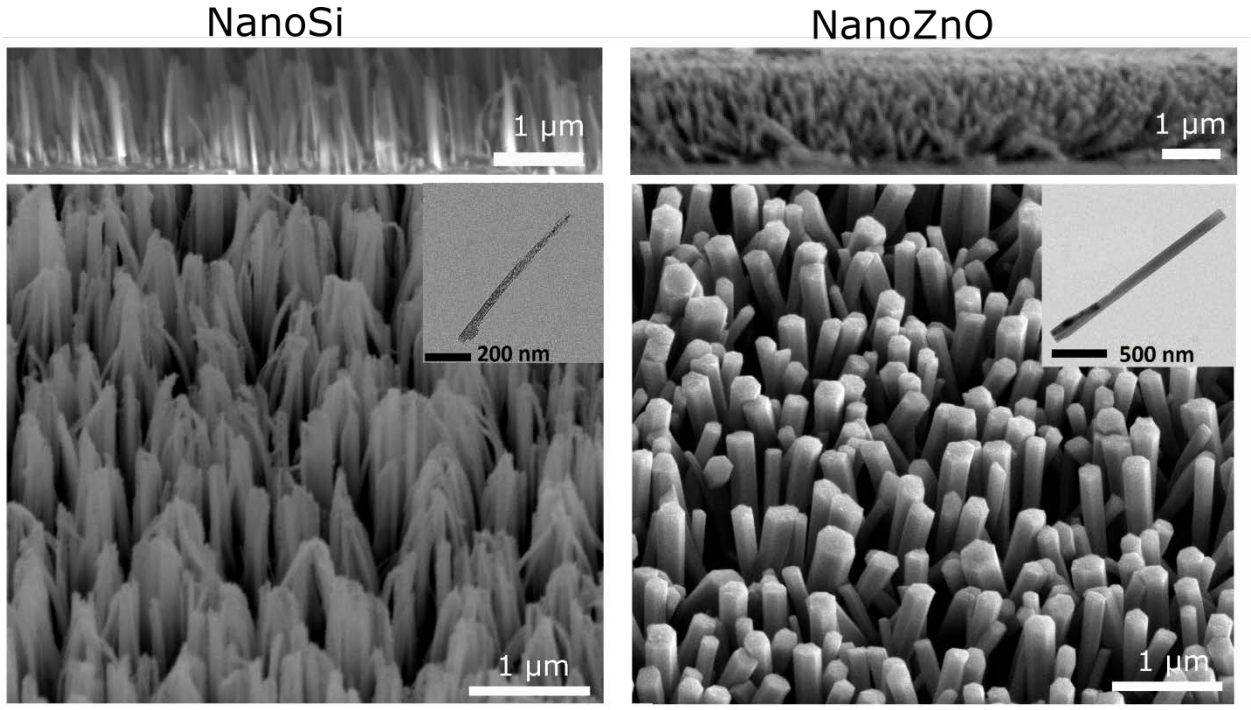

Fig. 1. SEM images of NanoSi and NanoZnO surfaces; side view (top), three-dimensional view (bottom). Inset shows a TEM image of one nanopillar. NanoSi consists of sharp vertical high-aspect ratio (diameter = 50 ± 10 nm, height = 0.9 µm) nanopillars and NanoZnO consists of multidirectional nanopillars with blunt-ends (diameter = 230 ± 65 nm and height = 1.2 µm). Nanopillars are randomly distributed on both NanoSi (spacing = 447 ± 395 nm) and NanoZnO (spacing = 408 ± 392 nm).

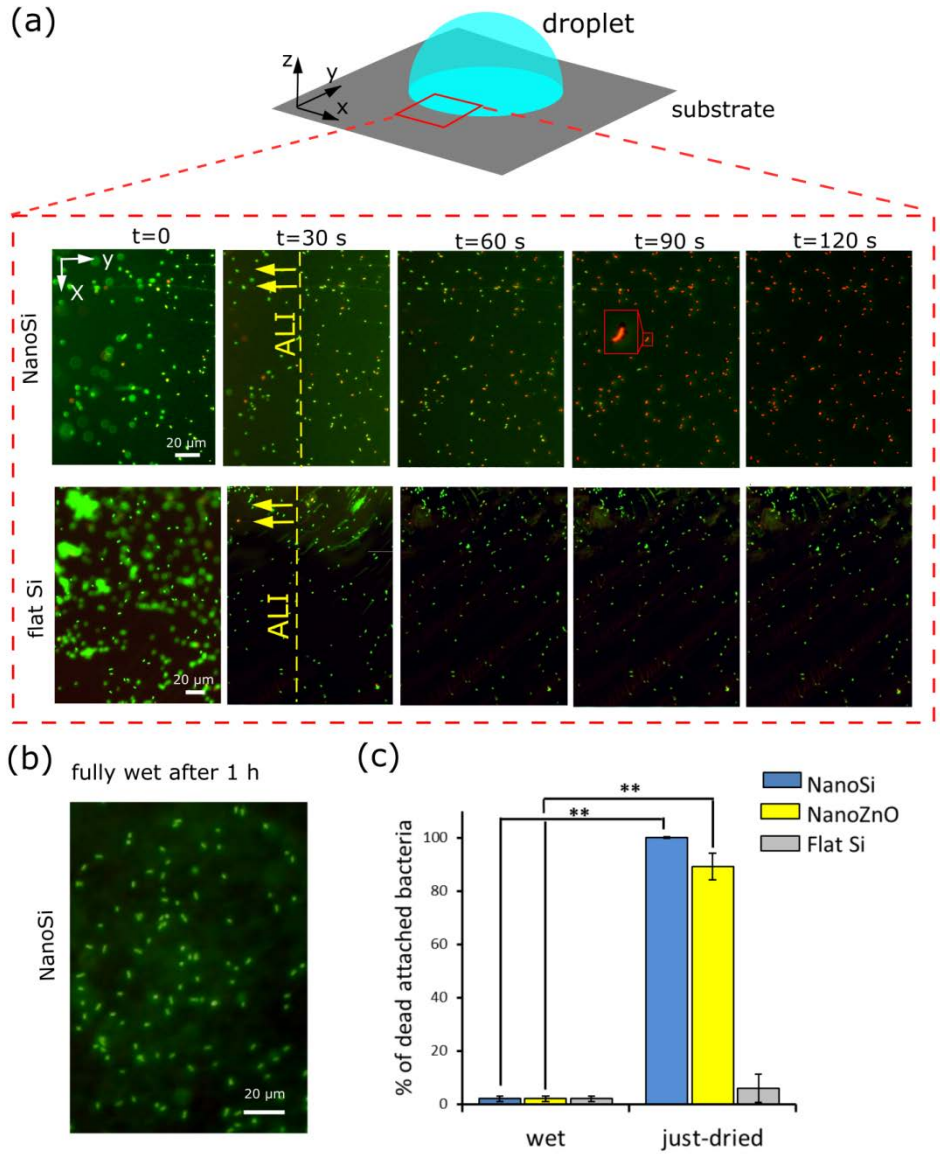

Fig. 2. *P. aeruginosa* viability on nanopillars and control (flat) surfaces upon evaporation. (a) viability of bacteria as a function of time on NanoSi and flat Si that is subject to evaporation (live cells are green and dead cells are red). A 3 μL droplet is placed on the surface and the air-liquid interface (ALI) was monitored during the last two minutes of evaporation. At t = 0, the surface is wet. At t = 30 s, the air-liquid interface is passing through the field of view (yellow line shows the approximate position of the ALI and the yellow arrow the of direction ALI movement). Images at t = 60 s and 90 s show the events that happen just after evaporation (inset at t = 90 s for NanoSi shows the magnified image of a bacterium after the film of water evaporates). At t = 120 s, the surface is completely dry. (b) bacterial viability in the immersed wet condition after 1 hr on NanoSi (for NanoZnO refer to Fig. S1) (c) Percentage of dead cells in the fully immersed wet condition, and immediately after evaporation of water on NanoSi, NanoZnO, and flat Si. Error bars denote the sample standard deviation and the experiments were repeated three times. **Statistically significant difference ($p < 0.05$, n = 3, Student's t-test).

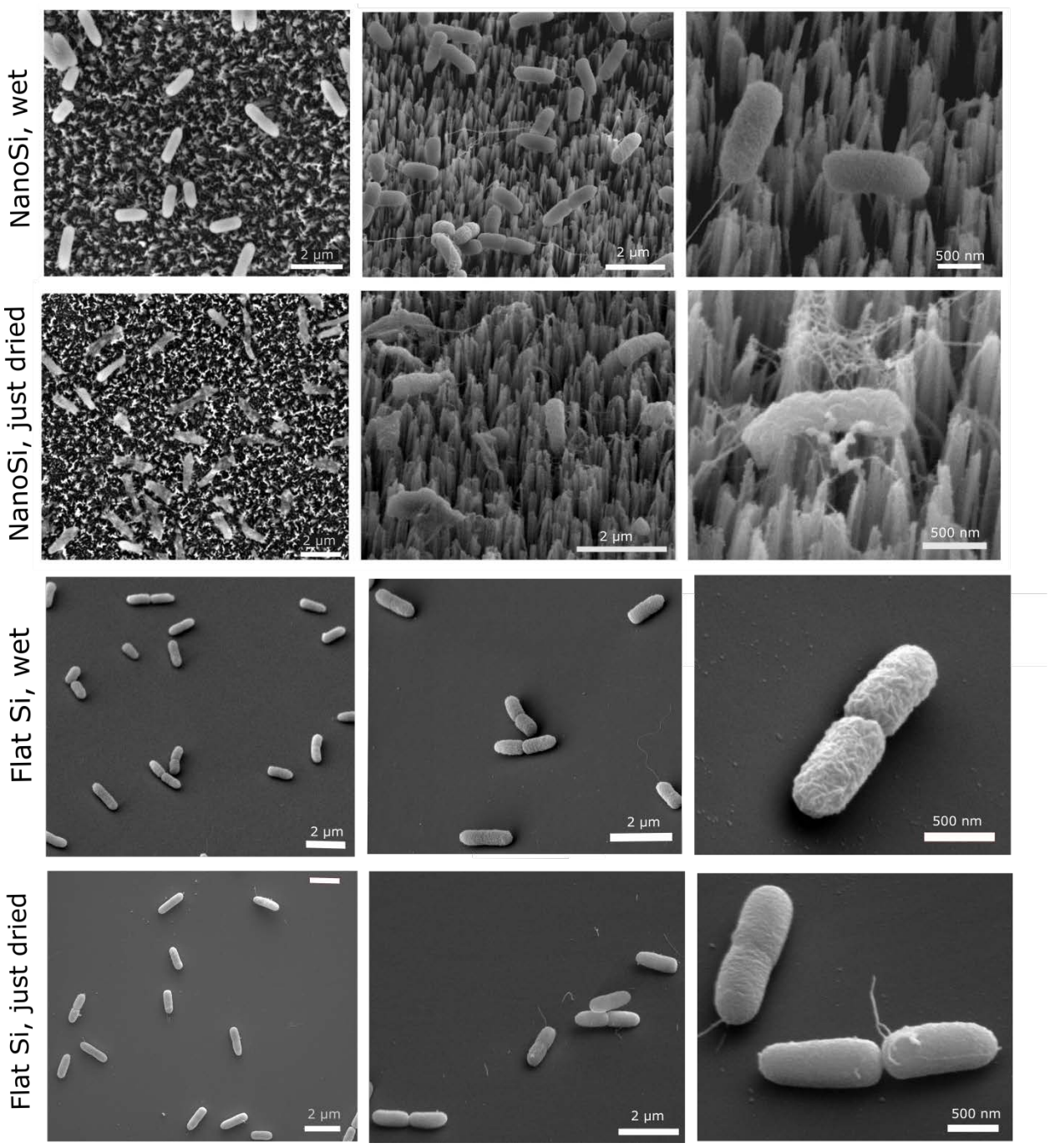

Fig. 3. SEM images of *P. aeruginosa* morphology on NanoSi and flat Si at the wet state (samples were not exposed to air, only chemically fixed and critical point-dried) and on NanoSi and flat Si just after water evaporation (samples were air-dried first and after complete water evaporation, chemically fixed and critical point-dried). For SEM images of NanoZnO refer to Fig. S5.

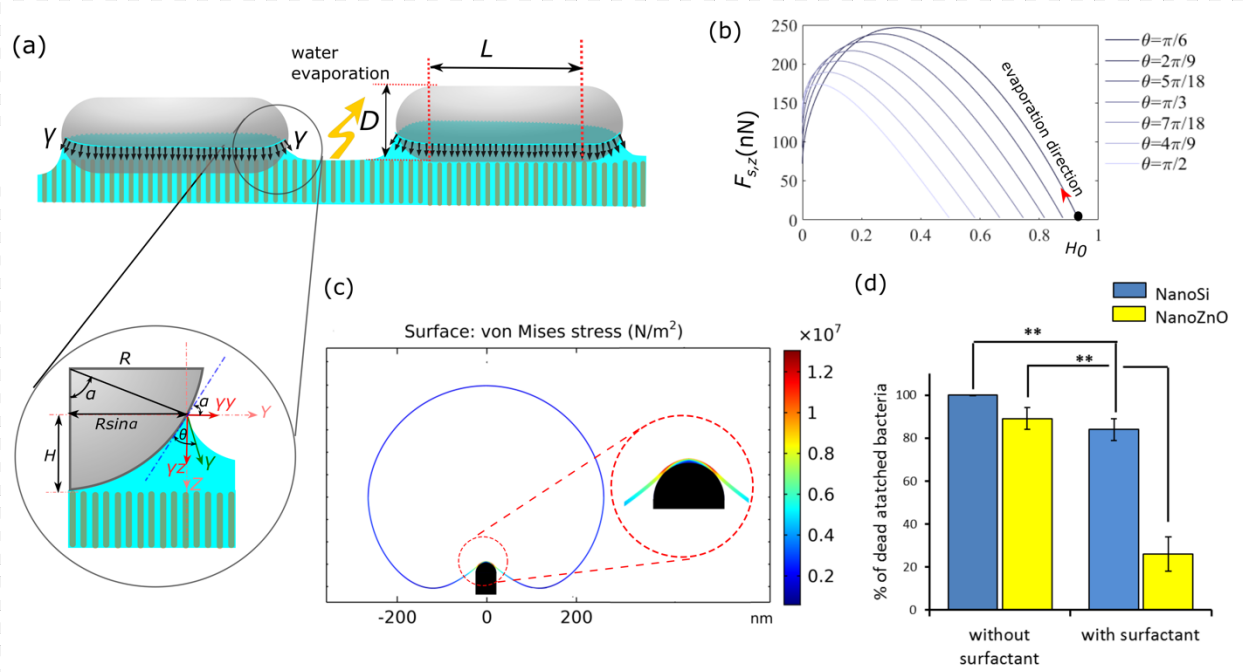

Fig. 4. (a) Sketch of the capillary meniscus on bacterium during water evaporation and analysis of capillary forces; (b) the magnitude of the surface tension force as a function of bacterial contact angle (θ) and the liquid level (H) during water evaporation (H_0 denotes the liquid level corresponding to initial equilibrium position of interface); (c) Numerical simulation of bacterial deformation in presence of an external force (F_{ext}) on NanoSi under the sticking-contact mode (refer to Fig. S7 for NanoZnO simulations, and Fig. S8 and Table S2 for non-sticking contact mode). The plots show the von-Mises stress profile on bacterial cell envelope. The external force was adjusted to give a maximum von-Mises stress of equal value to the cell wall ultimate tensile strength (for information about the simulation assumptions and parameters refer to SI); (d) Comparison of bacterial killing on NanoSi and NanoZnO in the absence and presence of Tween80. The viability of bacteria without surfactant is repeated from Fig. 1b. Error bars denote the sample standard deviation and the experiment for each treatment was repeated three times. **Statistically significant difference ($p < 0.05$, n = 3, Student's t-test).

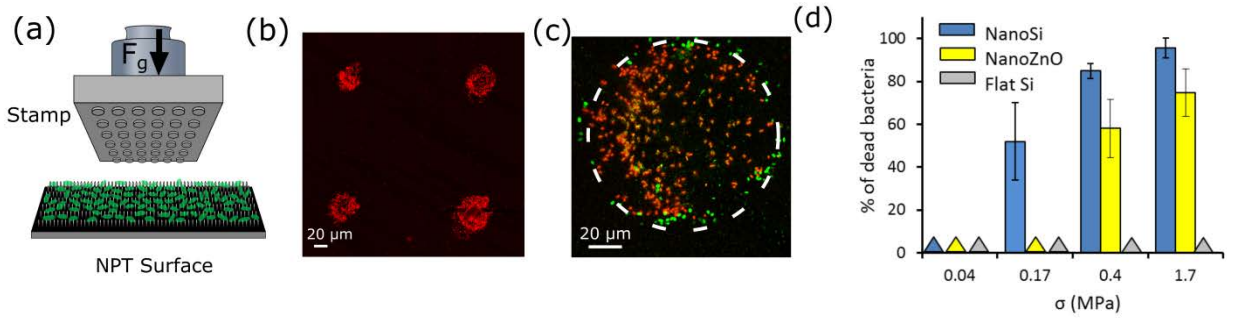

Fig. 5. Mechanical compression test: (a) sketch of an external gravitational force (F_g) applied by a 3D-printed stamp on bacteria attached to nanopillars; (b) kill-zone layout on NanoSi after the stamp contact at σ = 0.4 MPa; (c) dead and live bacteria in the kill-zone on NanoSi at σ = 0.4 MPa. The kill zone resembles the circular areas of microposts on the stamp (dashed line) (d) percentage of killed cells as a function of σ. Triangles represent the detection of no kill zone (i.e., all bacteria were viable). Error bars denote the standard deviations and experiments were repeated three times.

Graphical Abstract